

## Customizable cap implants for neurophysiological experimentation

Jackson D. Blonde<sup>a</sup>, Megan Roussy<sup>a,1</sup>, Rogelio Luna<sup>a,1</sup>, Borna Mahmoudian<sup>a</sup>,  
Roberto A. Gulli<sup>a</sup>, Kevin C. Barker<sup>a,b</sup>, Jonathan C. Lau<sup>c,d</sup>, Julio C. Martinez-Trujillo<sup>a,\*</sup>

<sup>a</sup> Cognitive Neurophysiology Laboratory, Department of Physiology and Pharmacology, Schulich School of Medicine and Dentistry, Robarts Research Institute and the Brain and Mind Institute, Western University, 1151 Richmond St. N., Room 7239, London, ON, N6A 5B7, Canada

<sup>b</sup> Neuronitek, 5846 William St., Lucan, ON, N0M 2J0, Canada

<sup>c</sup> Imaging Research Laboratories, Robarts Research Institute, Western University, 1151 Richmond St. N., London, ON, N6A 5B7, Canada

<sup>d</sup> Division of Neurosurgery, Schulich School of Medicine and Dentistry, Department of Clinical Neurological Sciences, London Health Sciences Centre, University Hospital, Western University, London, ON, Canada

### HIGHLIGHTS

- Implanted three rhesus macaque primates with novel, customizable PEEK cap implants.
- Each implant was acrylic-free.
- Reduced surgical invasiveness while increasing strength and utilizable surface area.
- Head fixation and chronic recordings were successfully performed.

### ARTICLE INFO

#### Article history:

Received 21 December 2017  
Received in revised form 9 April 2018  
Accepted 20 April 2018  
Available online 22 April 2018

#### Keywords:

Electrophysiology  
Macaque  
Customizable  
PEEK  
Cranial  
Implant

### ABSTRACT

**Background:** Several primate neurophysiology laboratories have adopted acrylic-free, custom-fit cranial implants. These implants are often comprised of titanium or plastic polymers, such as polyether ether ketone (PEEK). Titanium is favored for its mechanical strength and osseointegrative properties whereas PEEK is notable for its lightweight, machinability, and MRI compatibility. Recent titanium/PEEK implants have proven to be effective in minimizing infection and implant failure, thereby prolonging experiments and optimizing the scientific contribution of a single primate.

**New method:** We created novel, customizable PEEK 'cap' implants that contour to the primate's skull. The implants were created using MRI and/or CT data, SolidWorks software and CNC-machining.

**Results:** Three rhesus macaques were implanted with a PEEK cap implant. Head fixation and chronic recordings were successfully performed. Improvements in design and surgical technique solved issues of granulation tissue formation and headpost screw breakage.

**Comparison with existing methods:** Primate cranial implants have traditionally been fastened to the skull using acrylic and anchor screws. This technique is prone to skin recession, infection, and implant failure. More recent methods have used imaging data to create custom-fit titanium/PEEK implants with radially extending feet or vertical columns. Compared to our design, these implants are more surgically invasive over time, have less force distribution, and/or do not optimize the utilizable surface area of the skull.

**Conclusions:** Our PEEK cap implants served as an effective and affordable means to perform neurophysiological experimentation while reducing surgical invasiveness, providing increased strength, and optimizing useful surface area.

Crown Copyright © 2018 Published by Elsevier B.V. All rights reserved.

### 1. Introduction

Cranial implants are essential for non-human primate neurophysiological experimentation and their continual refinement enhances the well-being and potential scientific contribution of each primate. The rapid development of pre-fabricated cranial implants in recent years has motivated researchers to improve traditional techniques and materials and create safer, more effective, and more sustainable alternatives. These improvements are made

**Abbreviations:** PEEK, polyether ether ketone.

\* Corresponding author.

**E-mail addresses:** [jblonde3@uwo.ca](mailto:jblonde3@uwo.ca) (J.D. Blonde), [mroussy2@uwo.ca](mailto:mroussy2@uwo.ca) (M. Roussy), [rluna@uwo.ca](mailto:rluna@uwo.ca) (R. Luna), [bmahmou2@uwo.ca](mailto:bmahmou2@uwo.ca) (B. Mahmoudian), [roberto.gulli@mail.mcgill.ca](mailto:roberto.gulli@mail.mcgill.ca) (R.A. Gulli), [kevin@neuronitek.com](mailto:kevin@neuronitek.com) (K.C. Barker), [Jonathan.Lau@londonhospitals.ca](mailto:Jonathan.Lau@londonhospitals.ca) (J.C. Lau), [julio.martinez@robarts.ca](mailto:julio.martinez@robarts.ca) (J.C. Martinez-Trujillo).

<sup>1</sup> These authors contributed equally to this work.

<https://doi.org/10.1016/j.jneumeth.2018.04.016>

0165-0270/Crown Copyright © 2018 Published by Elsevier B.V. All rights reserved.

to two fundamental properties: implant design and implant material. Both factors are critical determinants of cranial bone, skin, and muscle health, which ultimately affects the comfort of the research animal as well as the longevity of the implant. Therefore, clear demonstration of improvements to animal welfare and experimental outcomes are important for justifying the substantial investment in time and money necessary to adopt a new technique (Adams et al., 2007).

Traditionally, cranial implants such as a headpost or recording chamber have been attached to the skull using anchor screws embedded in a cap of acrylic or dental cement (Lisberger and Westbrook, 1985; Mitz et al., 2009; Mueller et al., 2014; Pflugst et al., 1989). Acrylic does not bond directly to the skull but instead serves to hold the cranial implant to the anchor screws (Mulliken et al., 2015; Overton et al., 2017). Using acrylic in this way is fast, familiar, inexpensive, and well documented. In fact, Adams et al. (2011), found that 33/36 US primate visual laboratories that responded to their questionnaire had used the method of embedding both a chamber and headpost into a single acrylic cap. Though this material and technique are common, they are associated with adverse effects to bone, skin, and muscle health.

Acrylic undergoes an exothermic reaction when applied to the skull, releasing heat that may cause bone necrosis (Dunne and Orr, 2002; Eriksson and Albrektsson, 1983; Ormianer et al., 2000). Furthermore, because acrylic does not bind to the underlying bone directly, granulation tissue may form between the acrylic cap and skull, thus increasing the chance of the implant dislodging from the skull (Adams et al., 2011; Betelak et al., 2001; Mulliken et al., 2015). This risk is further enhanced by acrylic's cytotoxicity and lack of biocompatibility (Dahl et al., 1994; Treon et al., 1949). Acrylic is also difficult to mold intra-surgically; the outer surface of the acrylic cap may be left coarse with sharp edges at the skin border. These factors prevent skin healing, harbor infection, and make the cap difficult to clean (Adams et al., 2007; Adams et al., 2011). Lastly, after the acrylic cap has set, its surface cannot be utilized for experimental purposes (e.g. electrode pedestal or headpost attachment) unless an additional surgery is performed to cut the acrylic and access the skull. Taken together, acrylic can be biologically harmful and often compromises both the lifespan and stability of implants.

To circumvent the issues associated with acrylic, many groups have adopted alternative materials including stainless steel, titanium or plastic polymers such as polyether ether ketone (PEEK) for headposts and recording chambers. Titanium has gained popularity for these implant designs because of its mechanical strength, biocompatible coatings, customizability, and osseointegrative properties (Adams et al., 2007; Adams et al., 2011; McAndrew et al., 2012; Overton et al., 2017). Osseointegration refers to the process in which bone grows around the implant, increasing its durability and longevity (Buser et al., 1991; De Rezende and Johansson, 1993; Pflugst et al., 1989). Titanium is preferred over other metal alloys, such as stainless steel because of its lighter weight and lower elastic modulus, which is the ability to resist permanent deformation when a force is applied. If a material with an elastic modulus higher than bone is directly attached to the skull, the force shielding problem may occur. This refers to when a material absorbs and prevents the transmission of force delivered to a bone (Huiskes et al., 1992; Sagomonyants et al., 2008). Without force being continually transmitted to the skull, regular bone growth cannot occur and the bone under the cranial implant may degrade (Huiskes et al., 1992). Titanium has a lower elastic modulus than other metals, but its value may still be 6–20 times larger than cortical bone (Rho et al., 1993; Sagomonyants et al., 2008). This difference is large enough to cause force shielding. Another concern associated with titanium is its tendency to introduce MRI distortions (Mulliken et al., 2015;

Chen et al., 2017). Titanium creates shadows and distortions in the images, making subsequent brain navigation or electrode implantation inaccurate and potentially unachievable. There are also concerns regarding ion release from titanium, which may cause osteolysis (Niki et al., 2001). In contrast to titanium, PEEK has an elastic modulus closer to bone, is entirely MRI compatible, and does not corrode or release metal ions (Hunter et al., 1995; McAndrew et al., 2012). PEEK is also biocompatible, lightweight, and easily machined (Katzer et al., 2002; Sagomonyants et al., 2008).

The use of these strong acrylic alternatives has led to the development of implant footprint designs that cover smaller portions of the cranium, such as the K-headpost design (Adams et al., 2007; Adams et al., 2011; Chen et al., 2017; Lanz et al., 2013;). Ideally, after implantation the skin covers the legs while the protruding portion remains exposed and accessible. In older iterations, the legs were bent intra-surgically to conform to the shape of the skull. This process is laborious and frequently prone to error, resulting in an imperfect fit and a gap that is typically sealed with acrylic (McAndrew et al., 2012). To avoid intra-surgical bending, a mold of the skull may be taken ahead of time and subsequently used to create a model skull to bend the legs of the implant around (Betelak et al., 2001). Unfortunately, this process requires an additional surgery to expose the skull (Chen et al., 2017). As an improvement, researchers have recently used computed tomography (CT) or magnetic resonance imaging (MRI) techniques to non-invasively pre-form the feet of the implant to the skull, eliminating the need for manual bending (Chen et al., 2017; McAndrew et al., 2012; Mulliken et al., 2015). Together, these improvements have greatly enhanced implant stability and bone health when compared to acrylic caps. However, the main disadvantage of using 'legged' implants is the tendency for skin recession (McAndrew et al., 2012; Pflugst et al., 1989). Skin recession occurs because of the lack of bonding between the skin and the implant as well as the tension pulling the skin outward (Mulliken et al., 2015). As the skin recedes, the skull is gradually exposed, resulting in an open wound in which bacteria can be introduced, thus increasing the risk of infection. In these cases, the open area and exposed legs are typically covered with acrylic, incurring the adverse bone and skin effects previously mentioned, albeit at some delay.

To prevent skin recession, Mulliken et al. (2015) have developed form-fitted column implants that house the screw holes on the inside of the implant. As a result, the skin surrounding the column is directly bonded to the skull and does not recede. Though effective at preventing skin recession, Chen et al. (2017) have noted that concentrating the screws to one area of the skull reduces force distribution and increases the risk of the implant breaking from the skull. Furthermore, implants that sit higher off the skull, like the headpost shown in Mulliken et al. (2015), will experience more torque during head fixation. This is because the length of the lever arm (i.e. headpost), is directly proportional to torque when a force is applied perpendicular to the axis of rotation. This, combined with the fact that the headpost regularly receives substantial force, makes it a likely candidate for implant failure (e.g. breakage, dislodging from skull, failure to restrain head).

In the current study, we extend the tradition of cranial implant development in primate neurophysiology to improve the stability of implants and the health and longevity of research subjects. Using the workflow described here, we create customizable, skull-formed PEEK cap implants that facilitate better surgical pre-planning and simplify surgical procedures, while attempting to increase implant strength, reduce surgical invasiveness, and optimize the useable surface area of the skull.

## 2. Materials and methods

All surgical procedures and behavioural training were carried out in compliance with federal Canadian Council on Animal Care guidelines and Western University's Animal Care Committee guidelines. This committee serves as the active subcommittee of the Western University Council for Animal Care. All procedures are outlined in our Animal Use Protocol.

Three rhesus macaques (*Macaca mulatta*) were implanted with unique, skull-formed PEEK cap implants and either a PEEK or titanium headpost. Two of the three primates have also been implanted with a recording interface. Non-human primate (NHP) B (age 7), NHP T (age 9), and NHP M (age 5) were 9 kg, 13 kg, and 8 kg respectively at the time of the initial scanning. Fig. 1 shows a comprehensive overview of the cap design and implementation process.

Note that NHP T's implant was designed, manufactured, and implanted before NHP B and NHP M's implant. Therefore, we had the opportunity to refine the cap implant design and manufacturing procedures across the three primates, which reduced the total time required to create each implant. Only the differences between the three primates' implant designs or manufacturing procedures are explicitly stated; unstated details were unchanged. All figures referenced in Sections 2.3–2.7 pertain to NHP B. Section 2.8 outlines NHP T and NHP M's alternative implant designs.

### 2.1. Imaging data acquisition

In the current study, three unique cap implants were created. Though not always feasible, acquiring and co-registering both MRI and CT data ensures the most accurate surgical mapping and implant design because it combines high resolution images of the skull and brain. The cap implants for NHP B and NHP M were created using CT and MRI data, whereas the cap implant for NHP T was created using solely MRI data due to limitations of the scanner bore size.

MRI data were obtained using a 7T Siemens scanner (Centre for Metabolic Mapping, Robarts Research Institute, London, Ontario). The set of images chosen for NHP B, NHP T, and NHP M were MP-RAGE T1 sequence, 400  $\mu$ m isotropic (TE: 3.77; TR: 3000, FS: 6.98), MP-RAGE T1 sequence, 350  $\mu$ m isotropic (TE: 3.87; TR: 3000, FS: 6.98), and MP2-RAGE T1 sequence, 400  $\mu$ m isotropic (TE: 4.03; TR: 6500, FS: 6.98) respectively. Isotropic scanning is critical for accurate and reliable three-dimensional reconstruction of the skull and brain structures.

CT data were acquired using a GE eXplore Locus Ultra micro-CT scanner at the Robarts Research Institute (Western University, London, Ontario). Detailed imaging procedures are outlined in the supplementary materials.

### 2.2. Data pre-processing

Pre-processing of the MRI data began by importing the various 7T anatomical data sets (.ima format) into OsiriX Lite 7.5.1 (OsiriX, Switzerland; Rosset et al., 2004). The head of NHP B was not positioned straight in the scanner, causing the axis of orientation in OsiriX to be slightly misaligned with the subject's actual head. To correct this, a new set of images were generated in OsiriX by manually adjusting the axes to align with the head. Isotropic images are necessary for this correction. Images were then exported as a Digital Imaging and Communications in Medicine (DICOM) file format. Following exportation, the DICOM file was transformed to Neuroimaging Informatics Technology Initiative (nifti) format and image intensity non-uniformities were corrected using Advanced Normalization Tools (ANTs) N4 bias field correction tool. The nifti

file was then imported into Brainsight software (Rogue Research, Montreal, Canada).

The CT data acquired for NHP B and NHP M were converted from DICOM to Medical Imaging NetCDF (MINC) format and were subsequently imported into Brainsight.

The MRI and CT data for NHP B and NHP M were co-registered using MINC toolkit and a protocol designed in our lab. Manual landmark based co-registration was used in which the CT scan was registered to the target volume (MRI) using rigid body (6°-of-freedom) transformation. Co-registration is vital for mapping electrode implantation into underlying brain regions if the skull is to be used for implant design (McAndrew et al., 2012). Apart from its use in surgical pre-planning, co-registration was also used to compare the resolution of the skull between the two data sets. Fig. 2A shows transverse, coronal, and sagittal slices of the co-registered MRI (bronze) and CT (grey) data sets for NHP B. Green arrows in the figure indicate discrepancies in the skull between the two data sets. These discrepancies were considered minor enough to proceed with surgical mapping since the region of interest was on the superficial cortex. However, if the intended targets are deep within the brain, as was the case with NHP M, the discrepancies between the co-registered data sets must be corrected. The discrepancies were corrected for NHP M using a gradient distortion correction on the MRI data before co-registration. Further details regarding these corrections are outlined in Section 4.1 of the discussion.

### 2.3. Segmentation and skull reconstruction

Next, the MRI data (in the case of NHP T) and the co-registered CT data (in the case of NHP B and NHP M) were segmented to digitally reconstruct the skull. Segmentation refers to the process of labeling regions of interest in a data sample and was performed using Brainsight software. After importing the data into Brainsight, the anatomical data set was aligned based on the orientation of the animal in the scanner. Within the 'region of interest' tool, the intensity threshold of the voxels was adjusted to isolate the skull and delineate it from the surrounding tissue. Next, an automatic 'seed' tool was used to outline the skull slice by slice. After segmenting the entire skull, the 'reconstructions' tool was used to generate a three-dimensional reconstruction of the skull. Fig. 2B shows transverse, coronal, and sagittal slices of NHP B's segmented CT data as well as NHP B's reconstructed skull (orange).

### 2.4. Mapping of cap implant

After segmenting and reconstructing the surface of the skull, it was necessary to map out the desired locations of the various components for each cap implant. The objective for NHP B and NHP T was to implant microelectrode arrays (MEA; Blackrock Microsystems LLC, Utah, USA) into the prefrontal cortex. In contrast, the objective for NHP M was to implant deep brain electrodes into the amygdala (Ad Tech, WI, USA).

To begin, a three-dimensional, variable-depth rendering of the brain was created in Brainsight using the MRI data (Fig. 3A, left). On this reconstruction, target regions were identified using a combination of surface landmarks and a rhesus atlas co-registered to each NHP's MRI. The coordinates of these targets were then extrapolated to the surface of the digital skull reconstruction, providing a central point for the craniotomy during the electrode implantation surgery (Fig. 3A, right). A similar process is outlined in Johnston et al. (2016). These points then served as the location of either a removable panel (in the case of NHP B and NHP M) or chamber (in the case of NHP T) to be incorporated into the cap implant. A panel design was chosen for NHP B and NHP M to allow for a larger surgical field and the potential to change recording locations in the future.

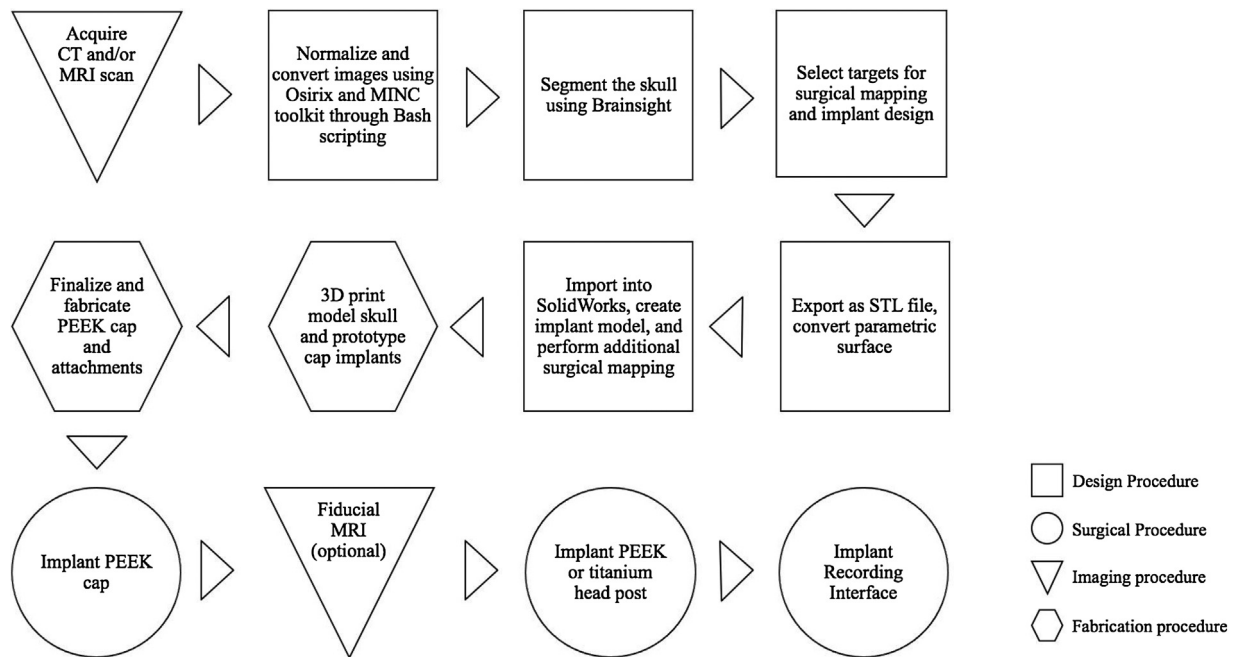


Fig. 1. Flow diagram of the cap design and implementation process.

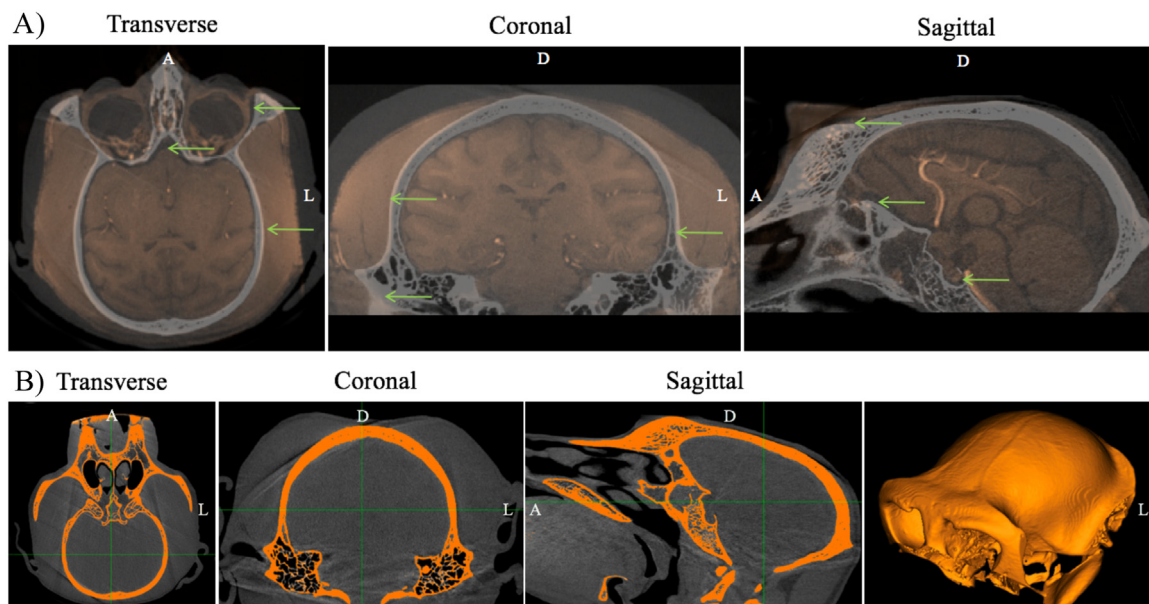


Fig. 2. A) Co-registration of the 7T MRI (bronze) and CT data (grey) of NHP B. Green arrows point to discrepancies in the skull between the two data sets. B) Segmentation and digital skull reconstruction in Brainsight using CT data from NHP B. The segmented skull is represented by the orange region. A=Anterior, D=Dorsal, L=Left. (For interpretation of the references to colour in this figure legend, the reader is referred to the web version of this article.)

Next, three coordinate points were selected along the midsagittal line of the skull in Brainsight. One point was selected at the skull's brow (anterior), one at the dorsal peak of the skull (central), and the third at the occipital protuberance of the skull (posterior; Fig. 3B). These three points created a reference of orientation of the digital skull in subsequent design software.

### 2.5. Digital design of cap implant

After selecting the coordinate points specifying the midsagittal line of the skull and the position of the anterior chambers/panels, the Brainsight data were exported as a stereolithography file (.STL). Since STL files represent triangular point clouds rather than solid

surfaces, aberrant folds and ridges are often hidden amongst the object reconstructions. The open-source software MeshLab was used to delete these aberrant ridges and folds as well as other unnecessarily complicated geometries such as those found within the nasal cavity (Cignoni et al., 2008). This resulted in a digital skull with a smooth and continuous curvature. This file was then converted from STL format to parametric surface format (.igs) using an inexpensive utility software (RhinoResurf, Rhinoceros 3D, Seattle, USA; McNeel, 2015).

Following conversion, the file was imported into SolidWorks (Dassault Systemes SolidWorks Corporation, Massachusetts, USA). There, the skull was used to create a digital prototype of the cap implant. First, a "bowl" of material was digitally superimposed over

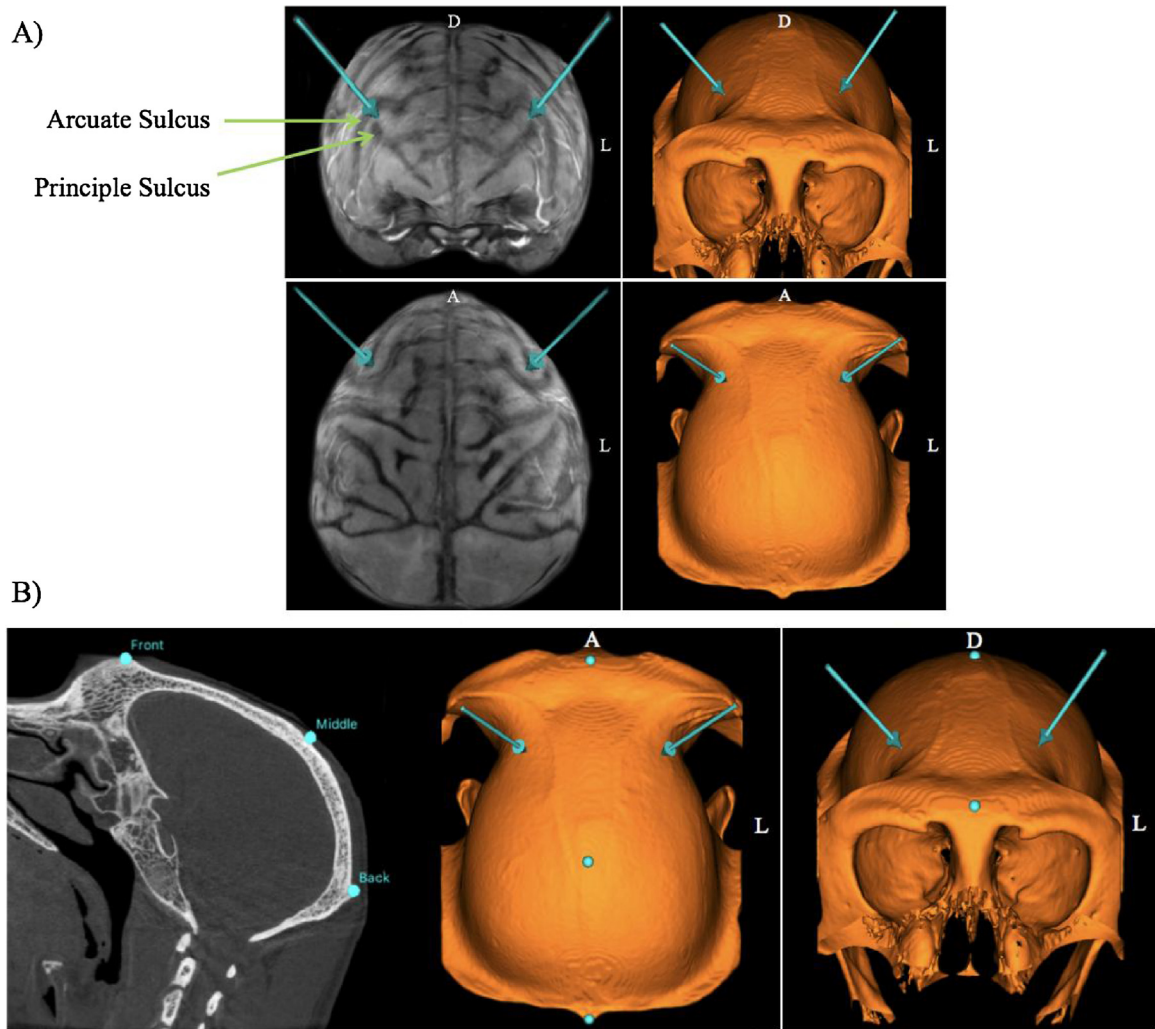
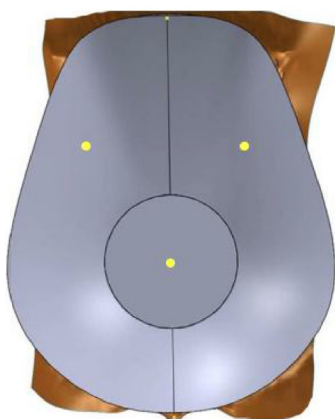
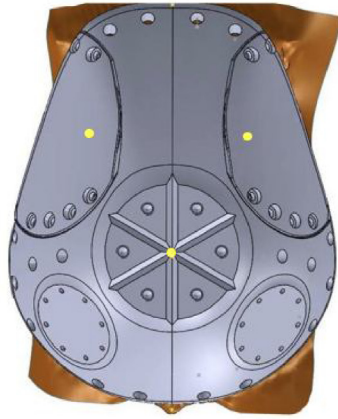


**Fig. 3.** A) Surgical mapping of the cap's removable panels (not shown) on NHP B using Brainsight. Left, brain surface reconstruction. Right, skull reconstruction. Blue arrows mark surgical regions of interest that were extrapolated from the surface of the brain to the surface of the skull. B) Selection of three midsagittal points on NHP B's skull. A = Anterior, D = Dorsal, L = Left. (For interpretation of the references to colour in this figure legend, the reader is referred to the web version of this article.)

1. Rudimentary Implant Design



2. Final Digital Prototype



3. Alternative View of Final Prototype



**Fig. 4.** Development of NHP B's digital prototype in SolidWorks. The underside of the implant was custom-fit to the surface of the digital skull (brown). Yellow dots indicate the location of the anterior panels and headpost baseplate. (For interpretation of the references to colour in this figure legend, the reader is referred to the web version of this article.)

the skull (Fig. 4, #1). From there, a cavity operation was performed to cut out excess material from the bottom of this object so that it conformed to the outer surface of the skull. The outer surface of the object was then modified to our desired specifications. Fig. 4 shows a progression from the rudimentary implant design (1) to the final digital cap implant prototype (2, 3) of NHP B. Note that there are various circular positions on the cap. These positions, hereafter referred to as “baseplates”, serve as the site of attachment of different components. The central baseplate is used to fasten a headpost onto the cap implant. The headpost is then used to fix the animal's head, which is essential for wired neural recordings and eye tracking. The two posterior baseplates are used to fasten MEA pedestals onto the cap implant. These pedestals provide an interface between the implanted MEAs and external hardware. The positions of the baseplates on the cap implant were not specified by coordinates and instead were chosen based on the available surface area on the model implant. The number of screw holes, their depth, and their positions on the cap were also chosen at this point. The remaining area of the implant was left blank to ensure a smooth and continuous surface to allow the skin to heal uniformly overtop. Approximately 8–10 h were required to draw and digitally assemble a finished cap.

In addition to the cap implant, it was necessary to design the attachments that would later be screwed directly onto the cap baseplates. For NHP B, these attachments included a headpost, anterior panels, baseplate covers, and the custom PEEK screws used to seal portions of the cap during healing. All attachments were designed in SolidWorks. Approximately 4 h were required to design the attachments.

Fig. 5 shows the design of NHP B's cap implant and the position of each component. Note that the cap shown is a 3D printed prototype (discussed in the next section) and not the final PEEK cap that was implanted.

## 2.6. Surgical mapping

After designing the cap implant in SolidWorks, the file was exported in Computer Aided Design (CAD) format. This was then imported into Brainsight and co-registered with the MRI or CT reconstructed skull. Recall that an MRI-reconstructed skull was used for NHP T's implant design and a CT-reconstructed skull was used for NHP B and NHP M's implant design. Fig. 6(1) shows NHP B's digital cap implant superimposed over its CT-reconstructed skull. This allowed for digital verification of the fit of the implant.

To perform surgical mapping of MEA wires from the surface of the brain to the MEA pedestals on the cap implant, the three-dimensional rendering of NHP B's brain from Fig. 3A (left) was then included in this co-registration. The digital skull was made transparent to visualize the underlying brain relative to the cap implant. Pathways (white) were then created to map the length and path of the wires connecting each chronic MEA to its recording pedestal (Fig. 6, #2 & 3).

## 2.7. Fabrication of the cap implant and attachments

As the cap implant for NHP B was designed in SolidWorks, some of the prototypes, their attachments, and a model skull were 3D-printed. Fig. 7 shows a progression from the digital skull (1) of NHP B to the final PEEK cap implant (4) using 3D printed models (2, 3). The models were printed using an EOSint printer (Krailing, Germany), which uses a laser sintering technique. As previous groups have shown, low-cost 3D-printed prototypes and other models can be used to evaluate the design and fit of the implant before a final implant is created using a costlier material (Lanz et al., 2013; Mulliken et al., 2015). Verification of the fit and functionality of the implant can be seen in Fig. 7(5,6). In these images, the front pan-

els of the implant have been removed, demonstrating the ability to access the surface of the skull quickly and efficiently. Additionally, the model headpost has been placed on the cap to demonstrate its attachment. The 3D-printed models were also useful for confirming where the desired baseplates, chambers, openings, and screw holes were to be placed.

After verifying the implant design using three dimensional digital models, the final PEEK cap and various attachments were manufactured. The SolidWorks files (SLD format) of the cap implant and attachments were first exported into a computer-aided manufacturing (CAM) program. This program was then used to guide a 3-axis computer numerical control (CNC) machine to cut the cap implant, baseplate covers, and MRI-compatible headpost from blocks of PEEK. Several laboratories have demonstrated effective fabrication processes using CNC machining (Adams et al., 2007; Lanz et al., 2013; McAndrew et al., 2012). The headpost used for head fixation was cut from a block of titanium using the same SolidWorks design and CNC machine. Since a 3-axis CNC machine was used, it was necessary to hand drill the screw holes that do not fall directly along the X, Y or Z axis. Various other small modifications were done manually, including tapping the screw holes and smoothing the edges of the implant. Ideally, a 5-axis CNC machine could be used to avoid some of these manual procedures. It took approximately 2–6 h to program the CNC machine and an additional 6 h to cut the cap implant out. Since we became more familiar with the machining protocols, this process took considerably less time for NHP B and NHP M's implants than for NHP T's implant.

## 2.8. Alternative cap implant designs

### 2.8.1. NHPT

NHP T's implant had a slightly different design than NHP B's implant, despite having similar objectives. Each coordinate point on the skull above the prefrontal cortex in NHPT was used as the center of a circular chamber instead of removable panel. The right chamber was designed to accommodate a conventional chamber used in acute or semi-chronic deep brain recordings. For these experiments, fiducial markers are required for online neuronavigation systems (Johnston et al., 2016). To this end, a fiducial post baseplate was positioned on the right posterior aspect of the implant. Fiducials were then fit to the cap to test the efficacy of fiducial registration in an MRI using our implant design. The fiducial baseplate was subsequently converted into a MEA pedestal baseplate via an adaptor (Fig. 8A). This simple modification allowed a single baseplate to be used for multiple purposes. Modifications to the baseplate were also possible while NHP T was head fixed, circumventing the need for an additional surgery. Furthermore, for NHP T, a trench was included between the left anterior chamber and the left posterior pedestal baseplate to house the MEA wire. The number of screw holes, their depth, and their positions on the cap were carefully designed. Fig. 8A summarizes the design of NHP T's cap implant and the intended position of each component. Note that the cap shown is a 3D-printed prototype and not the final PEEK cap.

During the digital design process, some of the prototypes, their attachments, and a model skull were 3D-printed using an Objet polyjet-based printer from Stratsys (Minnesota, USA). Fig. 8B shows a progression from the digital skull (1) of NHP T to the final PEEK cap implant (4) using 3D printed models (2 and 3). Verification of the fit and functionality of the implant can be seen in Fig. 8B (5,6).

### 2.8.2. NHP M

The implant for NHP M was designed to allow for the insertion of deep brain electrodes into the amygdala. To this end, a large chamber was included in the anterior portion of the implant. This allowed for flexibility in the planning of the trajectory as well as the

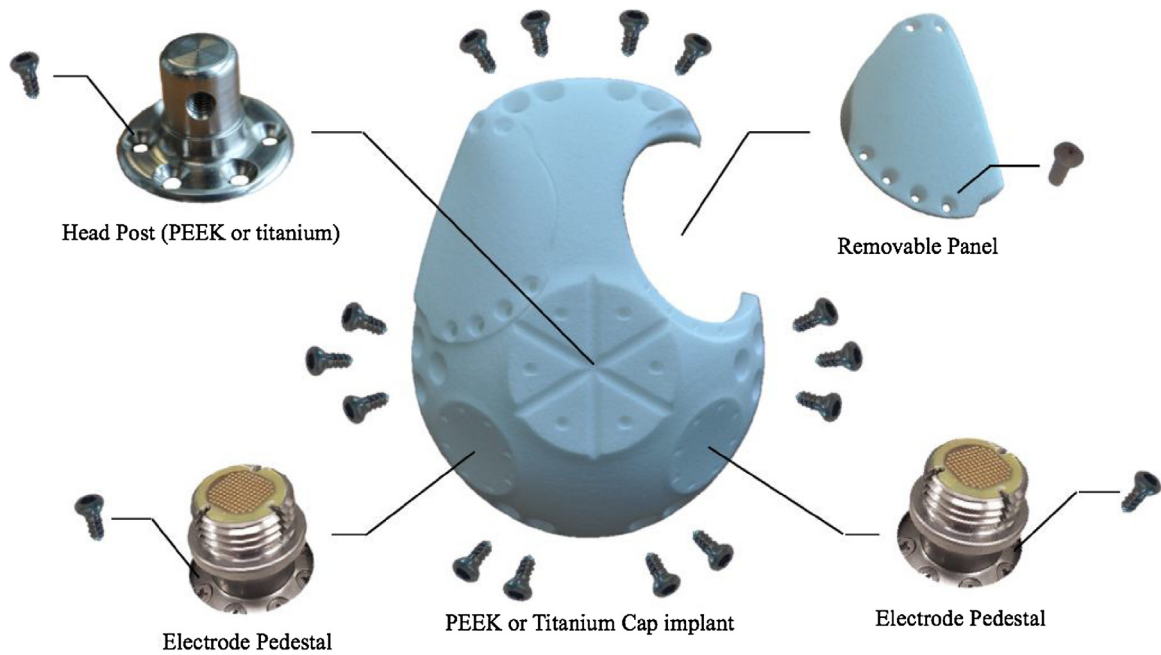


Fig. 5. Schematic breakdown of a prototype cap implant and parts for NHP B.

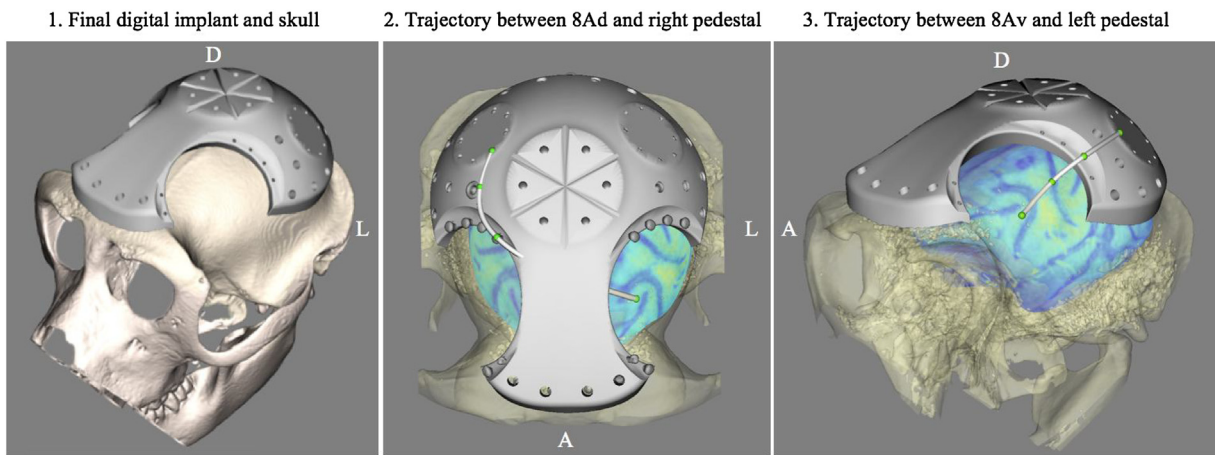


Fig. 6. Surgical mapping of microelectrode array implantation for NHP B. A = Anterior, D = Dorsal, L = Left.

potential to change recording locations in the future. To allow for head fixation, a headpost baseplate was included in the posterior portion of the implant.

To verify the fit and functionality of the implant, a model skull, prototype implant, and implant accessories were 3D-printed using an Objet polyjet-based printer from Stratsys (Minnesota, USA; Fig. 9, #1 and 2). Removing the front panel allows for the attachment of custom-designed guides that can flexibly change the recording location (white construct, Fig. 9, #1). A steel bone screw fits into the guide and holds the macroelectrode stably in place. To house the electrode connector safely between sessions while the animal is in its home cage, a cylindrical compartment is attached to the chamber and sealed with a lid (Fig. 9, #2; compartment lid not shown). The final 3D-printed PEEK cap implant is shown in Fig. 9, #3.

### 2.9. Cap implantation

This section describes the nuances of the cap implant procedure for NHP B, NHP M, and NHP T respectively. See the supplementary materials for a detailed description of the cap implant procedure.

For NHP B and NHP M, a semi-circle incision around the perimeter of the head was used to expose the skull (Fig. 10, #1). There were no visible gaps between the cap implant and skull, indicating a proper fit (Fig. 10, #2). Titanium and stainless steel screws were used to attach the implant to the skull. However, ceramic screws can be used if there is a need for a subsequent MRI. The baseplate and chamber covers were attached to the implant using PEEK screws. The duration of the surgery was 4 h and the skin was completely sealed over the implant (Fig. 10, #3 & 4).

For NHP T, a triangular incision was used. There was a visible gap between the anterior portion of the implant and the skull, which indicated an improper fit. However, this gap was small and we proceeded with the implantation. Ceramic bone screws were used to fasten the implant to the skull. Ceramic screws allowed the cap to remain fully MRI compatible, which was required for this animal. The baseplate and chamber covers were attached to the implant using PEEK screws. The duration of the surgery was 4 h and the skin was completely sealed over the implant.

We did not document any differences in the stability of the implant between the three animals. Thus, we assume that both ceramic and titanium/stainless steel screws are sufficient to hold

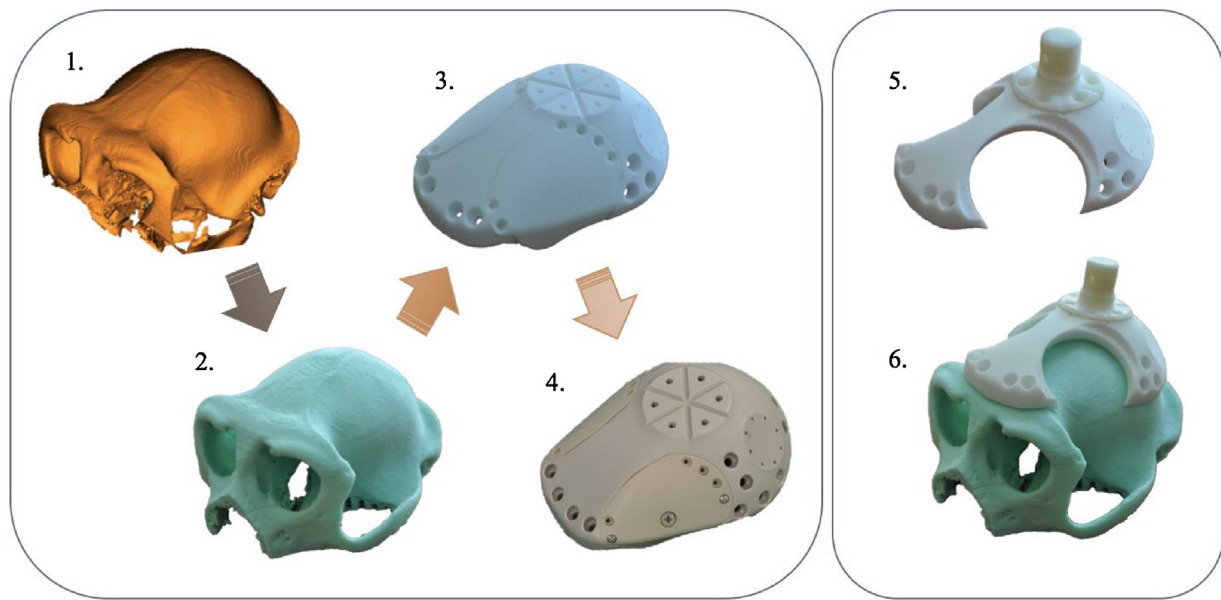


**Fig. 7.** Progression of NHP B's cap implant design from digital skull (1) to the final PEEK cap (4) using 3D-printed models (2,3). Verifying the functionality and fit of the implant, headpost and access to surgical field (5,6).

the implant to the skull. The screw choice depends primarily on the need for MRI-compatibility and cost. Ceramic screws are slightly more expensive than titanium and stainless steel screws and require greater care when tightening because their screw heads are more brittle.

#### 2.10. Post-Implant CT and MRI scans

A CT and MRI scan were taken following cap implantation for NHP B/NHP M and NHP T respectively. These scans followed the procedures outlined in the supplementary materials and were used to verify the fit of the implant on the skull. The set of MRI images chosen for NHP T was MP-RAGE T1 sequence, 430 m isotropic (TE: 3.13; TR: 2500, FS: 6.98). Since stainless steel and titanium screws were used to fasten NHP B and NHP M's implants, a CT scan was taken.

#### 2.11. Headpost attachment

See the supplementary materials for a detailed description of the headpost attachment procedure. First, an oval-shaped elliptical incision was made on the skin above the baseplate cover (Fig. 11, #1), which was the same size as the headpost diameter. The skin was pulled back to each side to reveal the headpost baseplate (Fig. 11, #2). The PEEK cover over top of the headpost baseplate was removed and replaced with a titanium headpost for NHP B and NHP M and a PEEK headpost for NHP T. The titanium headpost was attached using 6 titanium screws. The PEEK headpost was attached using 6 PEEK screws, making NHP T's implant fully MRI compatible. The skin was then sutured around the headpost (Fig. 11, #3). The duration of the procedure was less than 1 h.

### 3. Results

#### 3.1. Post-Implant CT and MRI scans

The CT scans for NHP B and NHP M following cap implantation revealed a close fit of the implant over the skull (Fig. 12). Distortions caused by the titanium and stainless steel screws can also be seen

in the CT images. The MRI scan for NHP T revealed a continuous layer of granulation tissue between the skull and implant (Fig. 12).

#### 3.2. Skin recession and infection

The skin was initially sealed over the cap implant in NHP B. In the following week, seroma began to form between the implant and the fascia tissue. To avoid discomfort that this may cause the animal, a sterile procedure was performed under general anesthesia to drain the fluid. The fluid was then subsequently tested for infection using a culture test and no infection was detected. The wound healed and full hair growth was present three months later (Fig. 10, #5). Seroma also formed between NHP M's implant and sealed fascia tissue; however, the seroma was small and was reabsorbed within a week after the surgery.

Following headpost implantation in NHP T, the skin progressively receded to the border of the implant. Continual cleaning of the skin border was then required. To avoid this in NHP B and NHP M, the recessed surfaces found on NHP T's cap design were removed for NHP B and NHP M's cap design. No skin recession was reported in NHP B or NHP M following headpost implantation. The skin remained at the base of the headpost and was free of infection or inflammation (Fig. 13).

#### 3.3. Head fixation

Head fixation has been successfully performed on NHP B and NHP M for eight months and one month respectively (Fig. 13). Head fixation during behavioural training for NHP T was initially performed using a PEEK headpost and PEEK screws. Approximately 1 month after head fixation training had begun, NHP T jerked and broke the PEEK screws holding the PEEK headpost to the cap. The headpost was no longer attached to the cap but was structurally intact. A short procedure was then performed to remove the broken screw shafts from the cap and attach a titanium headpost with titanium screws. Both a titanium headpost and titanium screws were used due to their superior strength; however, a PEEK headpost with titanium screws was also tested and was found to be adequately resilient. After the procedure, head fixation was successfully per-

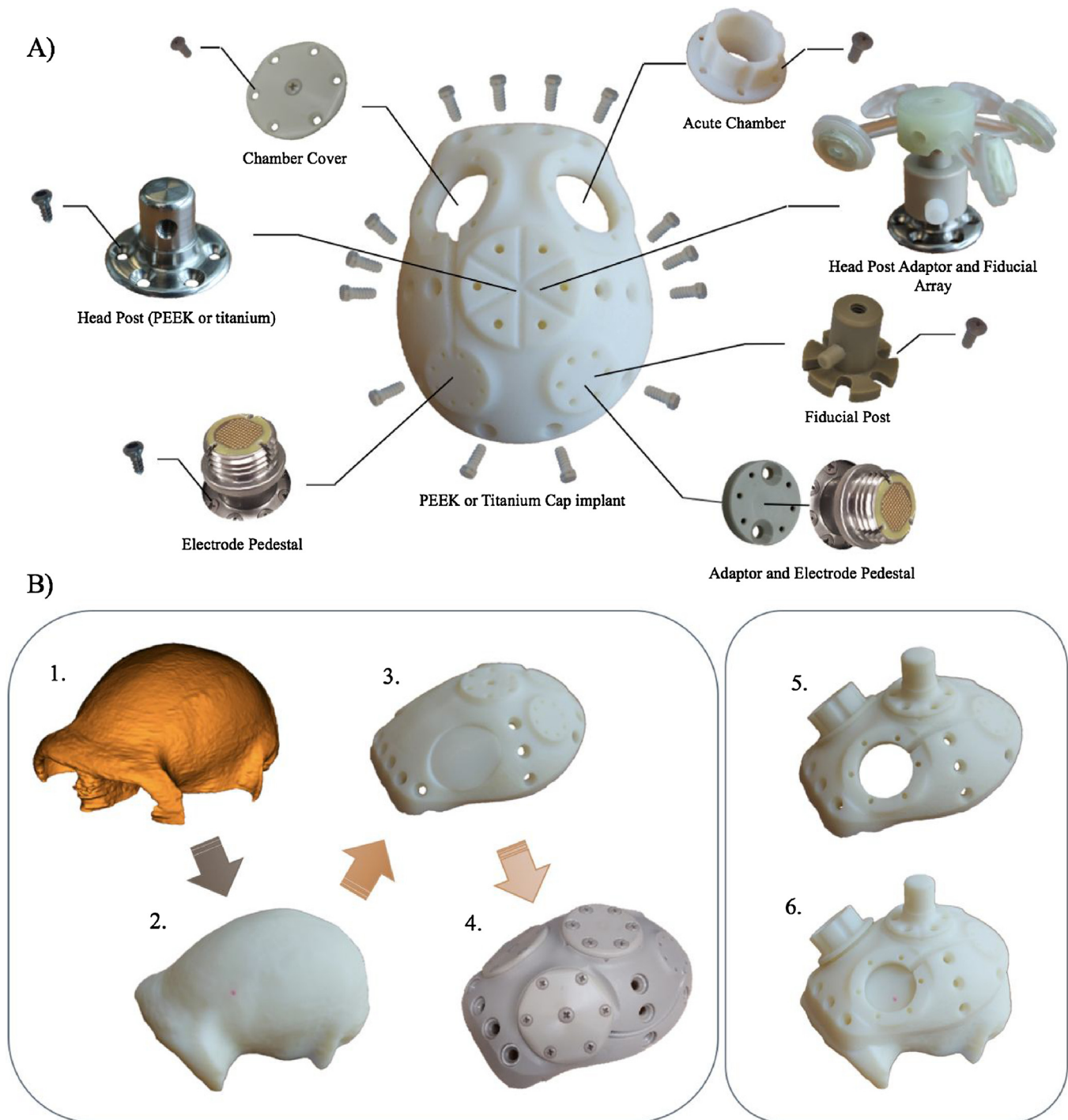


**Fig. 8.** A) Schematic diagram of a prototype cap implant and parts for NHP T. B) Progression of NHP T's cap implant design from digital skull (1) to the final PEEK cap (4) using 3D printed models (2,3). Verifying the functionality and fit of the implant, headpost and access to surgical field (5,6).

formed for 12 months. Taken together, we do not recommend attaching the headpost to its baseplate using PEEK screws.

#### 3.4. Installing recording interfaces

To subsequently implant recording interfaces in NHP B and NHP T, the skin covering the cap had to be removed so that the chambers/panels and MEA pedestals were exposed. This process was faster for NHP T because the skin had already receded to the edge of the cap implant. Following removal of the skin, the implants resembled acrylic caps; however, the different elements (i.e. cap surface,

chambers, screws, baseplates) were more biocompatible and easier to access and modify than an acrylic cap. Continual cleaning of each implant and skin border was required for the duration of each project. Cleaning the PEEK cap was significantly easier than cleaning an acrylic cap because of its smooth and uniform surface. Furthermore, the skin and muscle that were in direct contact with the PEEK cap remained clean and free of infection (Fig. 10, #6).

Two MEAs were successfully implanted in areas 8Ad and 8Av of the left hemisphere of NHP T and NHP B. For NHP T, an MEA baseplate adaptor was attached on to the fiducial baseplate in the right posterior portion of the implant (Fig. 8A). Grooves were carved into



**Fig. 9.** NHP M cap implant design. (1, 2) 3D-printed prototype and model skull to verify the fit and functionality of the implant. (3) Final PEEK implant with front panel in place.

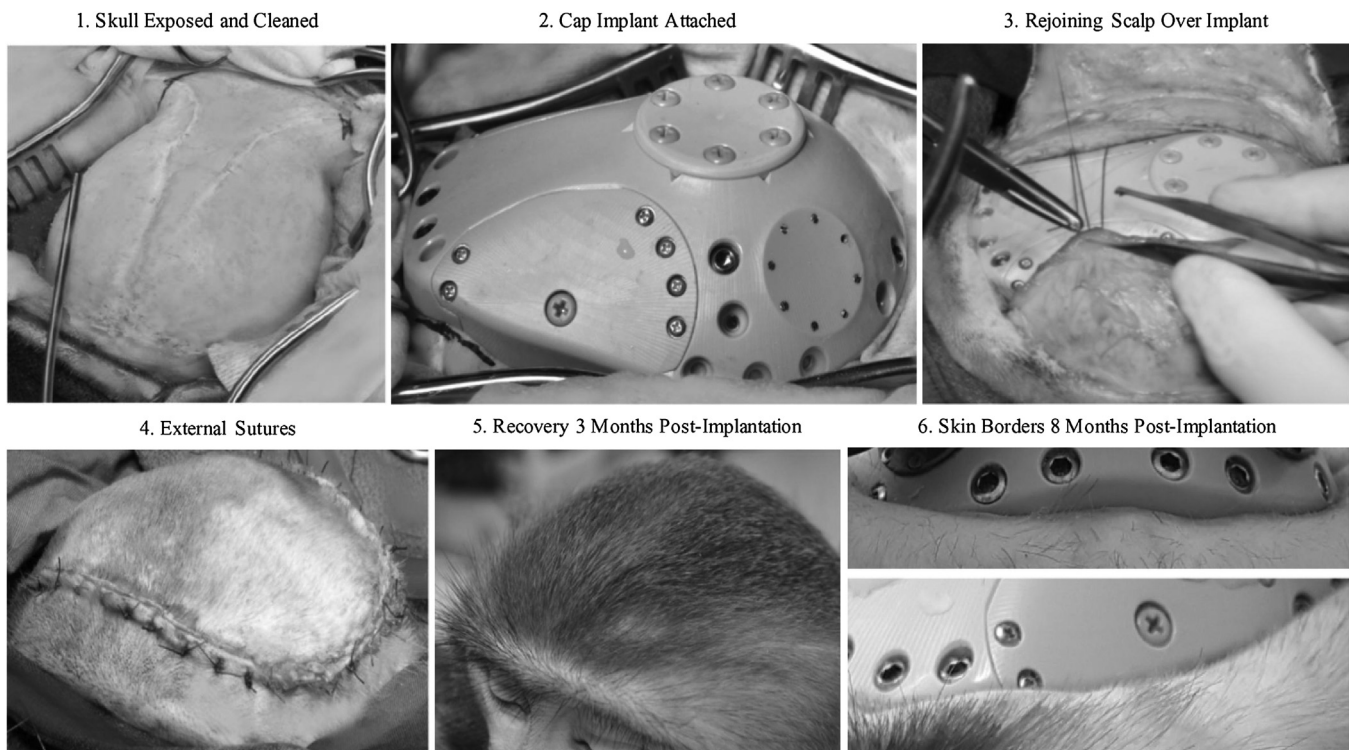


**Fig. 10.** Cap implantation procedure.

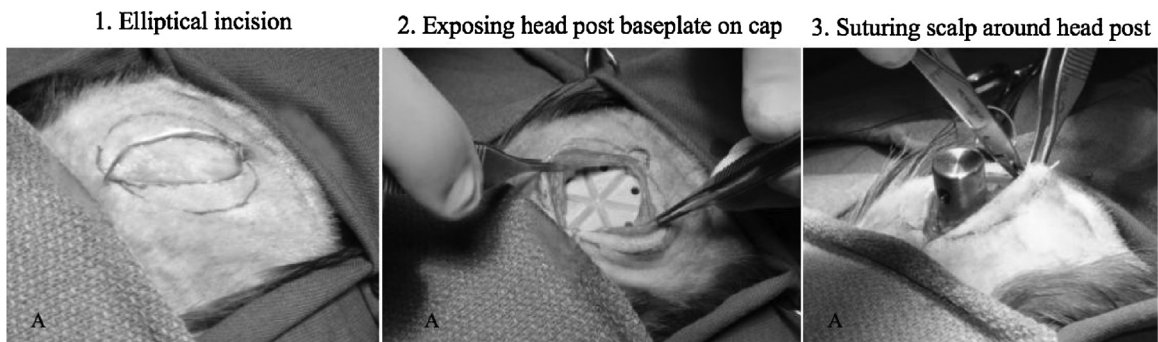


**Fig. 11.** Headpost implantation procedure. A = Anterior.

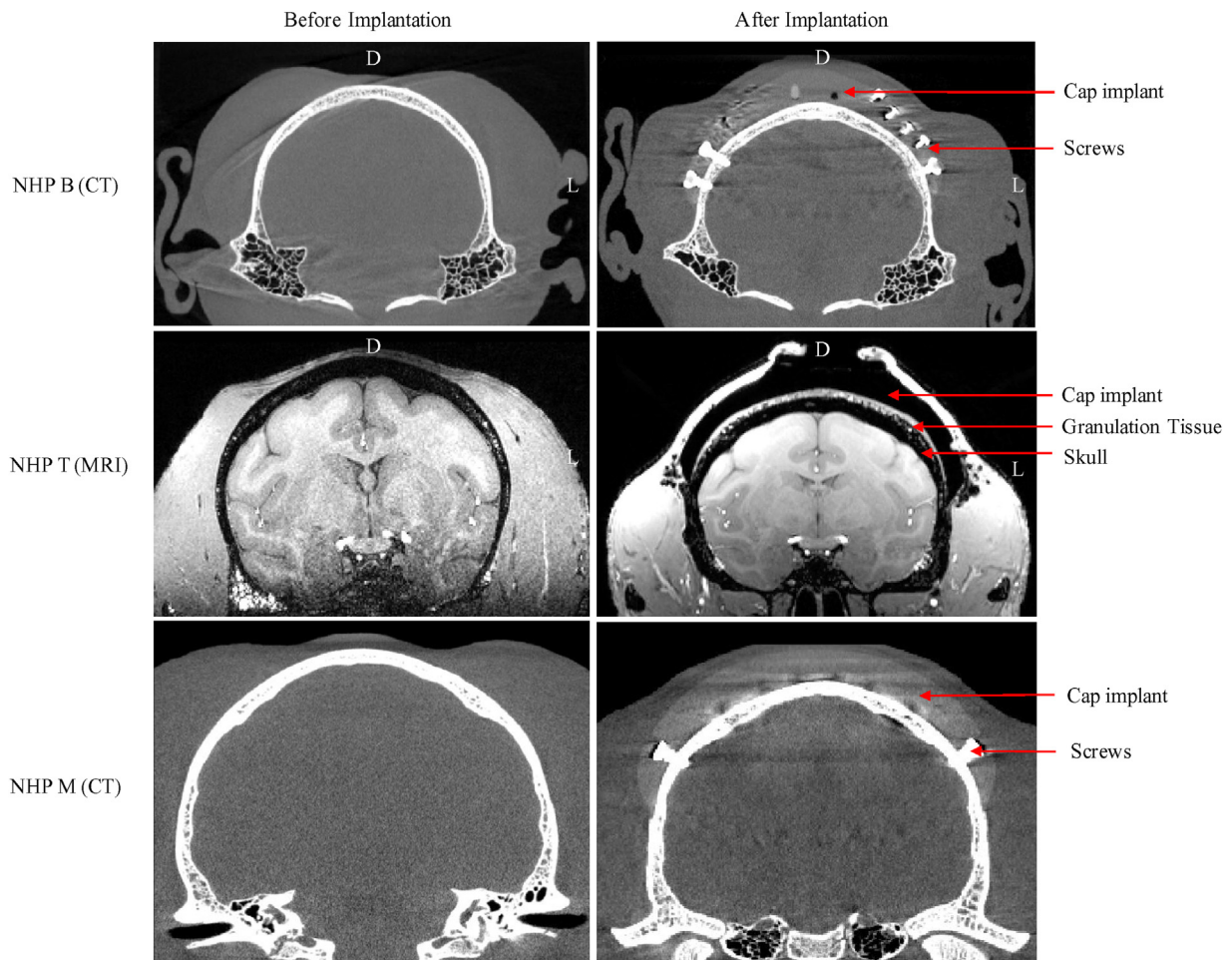


**Fig. 12.** CT and MRI images preceding and following NHP B, NHP T, and NHP M cap implantation. D=Dorsal, L=Left.



**Fig. 13.** Head fixation to be utilized during eye tracking and behavioural training. NHP B's head has been shaved at the base of the headpost, revealing healthy skin free of infection or inflammation.

the surface of each cap to house the MEA wires. Acrylic was applied to the surface of the cap to embed the MEA wires and pedestals, which prevented the animals from picking at the hardware. Chronic recordings were successfully performed on NHP T and NHP B for 6 months and 5 months respectively. Recordings from NHP B are ongoing. A recording interface has not yet been implanted in NHP M and the skin remains at the base of the headpost.

#### 4. Discussion

Our novel cranial implant design resembles the “skull caps” used in [Betelak et al. \(2001\)](#), except that our implants do not use acrylic, are created using imaging data, and are installed in one surgery. Installing the cap in one surgery allowed all subsequent surgeries to occur quickly and with minimal invasiveness. In contrast, attaching multiple independent legged or column implants to the skull requires several more invasive procedures. The overall number of screws used to fasten each implant to the skull was also reduced. For example, attaching the headpost and chamber shown in [\(Chen et al. \(2017\), Fig. 8\)](#) would require a total of 29 screws. In contrast, the cap implant used for NHP T in the current study required 14 skull screws and had capacity for two chambers, two MEA pedestals, and a headpost. Furthermore, implanting multiple individual attachments would occupy a similar surface area as our cap implant [\(Chen et al., 2017\)](#). Therefore, we skip this prolonged and more invasive process and introduce a cap in a single surgery. Though our implants cover a large surface area, we believe that reducing surgical invasiveness is worthwhile. Consequently, our design is

optimal for projects that require multiple components to be fastened to the skull, which may become more frequent with the need to record from multiple brain areas (e.g., [Mendoza-Halliday et al., 2014](#)), while using chronic MEA recordings ([Tremblay et al., 2015](#); [Leavitt et al., 2017](#)), deep brain recordings, or when conducting recording and inactivation experiments simultaneously.

So far, our design has been implemented in projects in which the brain area to be recorded from or manipulated is known ahead of time. However, in many current primate studies, it cannot be known where to place a chamber or array before the headpost surgery. To extend our implants to these studies, we are developing a variation on our design in which a PEEK, custom-fit “ring” is first implanted around the periphery of the skull ([Fig. 14](#)). From there, different PEEK caps can be screwed to the ring. The first PEEK cap installed to the ring can be designed with a built-in headpost so that awake functional MRI imaging can be used to determine areas of interest following task performance. This cap can then be subsequently unscrewed and replaced with a cap containing chambers, pedestals, or other desired hardware ([Fig. 14](#)).

Additional advantages of our cap implant design include: avoiding the use of acrylic, increased force distribution, full customizability, and surgical pre-planning. The cap implant itself was composed of PEEK and was directly screwed to the skull. This circumvented the need for acrylic and anchor screws, which allowed us to avoid various issues associated with acrylic, including: heat-induced bone necrosis, lack of skull adhesion, and time consuming intra-surgical application ([Dunne and Orr, 2002](#); [Adams et al., 2011](#)). Alternatively, some primate laboratories have reported using adhesive resin cements, such as C&B Metabond (Parkell, Inc., Edgewood, NY, USA) to prevent granulation tissue formation and to increase acrylic’s adhesion to the skull ([Dotson et al., 2017](#); [Nummela et al., 2017](#)). These cements are usually applied as an interface between the skull and acrylic cap. Dental literature suggests that C&B Metabond (4-META/MMA-TBB) is biocompatible, strong, and highly adhesive ([Chang et al., 2002](#); [Nakagawa et al., 2015](#)). Although the addition of C&B Metabond appears to be an improvement on “acrylic only” implants, it increases surgery times (it must be mixed, applied, and cured) and does not prevent the formation of an acrylic-skin border that is irregular and thus prone to infection. Furthermore, once the resin cement has bonded to the skull, removing it becomes difficult ([Borden et al., 2017](#)). This prevents researchers from easily changing recording locations or installing subsequent implants. Our design resolves these issues by reducing surgical times, creating a clean interface between the implant and skin ([Fig. 10, #6](#)), and having the potential to be easily removed from the skull by removing the screws. Furthermore, NHP M’s implant ([Fig. 9](#)) and our new prototype design ([Fig. 14](#)) increase the amount of accessible skull, which allow us to flexibly manipulate different brain regions over time. Lastly, the accessories used for recordings and immobilization of the head in our implant design (e.g. headpost, chambers, pedestals, etc) are not directly attached to the skull, but instead to the cap implant. Therefore, they can easily be removed and replaced, which would not be the case if they were attached to the skull using adhesive resin cement.

The PEEK material also proved to be highly biocompatible and easy to clean. The large surface area of our implant also increased force distribution and reduced the likelihood of the implant dislodging from the skull. The customizability of our design was apparent as each cap was pre-designed with various chambers and baseplates specific to the project’s needs. Allocating the positions of components ahead of time also optimized useful surface area and allowed us to perform surgical pre-planning. Using the digitally designed implant, reconstructed skull, and three dimensionally rendered brain, we mapped out electrode implantations and the positions of craniotomies ([Fig. 6](#)). This increased the efficiency of the surgeries and helped to minimize invasiveness. It is

important to note that many of the results supporting these claims are qualitative and based on visual observation by researchers and veterinarians.

Lastly, our implants were affordable, costing approximately \$2000 (CDN) for each cap implant and its attachments. The PEEK material and labor cost \$400-500 and \$1500-1600 respectively. This cost included the use of various purchased software packages. If the design and fabrication process were substituted with open-source software, like in [Chen et al. \(2017\)](#), the overall cost would be reduced. This would also make the design process more accessible to other primate researchers.

#### 4.1. Limitations

Despite the overall success of the cap, some complications arose from NHP T’s implant including an imprecise fit to the skull and a headpost screw breakage. Fortunately, the causes of these complications were identified and our methodology was updated accordingly for NHP B and NHP M. The improper fit of the cap implant on NHP T resulted in a gap between the skull and implant that provided room for a small amount of granulation tissue to grow ([Fig. 12, middle](#)). This was likely due to a combination of poor cortical bone contrast in the MRI used for skull reconstruction and geometric distortion. Though 7T MRI provides increased spatial resolution of brain tissue relative to 3T MRI, which was exploited for surgical mapping in the current study, it may also result in greater distortion. [Fig. 15](#) compares the distortions between 7T and previously collected 3T data for NHP T using the pipeline described in [Lau et al. \(2018\)](#). The differences in distortion between the two data sets ranged from 2 mm (red) to 4 mm (yellow), depending on the brain area. Some of these distortions are associated with gradient field inhomogeneity, which increase in tissues that are farther from the center of the magnetic field, such as the skull ([Lau et al., 2018](#)). Therefore, these distortions may decrease the accuracy of a digitally reconstructed skull generated from MRI data. It is important to note that gradient field inhomogeneity distortions do not worsen with increased magnetic field strength and may be corrected using manufacturer-provided or post-processing algorithms. Main field distortions ( $B_0$ ) also contribute to the distortions seen in [Fig. 15](#). These distortions are harder to correct for and increase closer to air-tissue interfaces. Ultimately, the distortions associated with 7T MRI compromise the accuracy of the digital reconstruction of the skull as well as the subsequent fit of the implant, as we observed in our study.

Importantly, the granulation tissue that resulted from the imprecise fit remained sealed under NHP T’s implant and did not compromise the stability of the cap. In fact, the implant remained stable for the duration of the project (14 months). This highlights the strength and biocompatibility of our cap implant design. Although the granulation tissue was not problematic, it is known to increase the likelihood of infection, bone degradation, and implant failure ([Chen et al., 2017](#); [Johnston et al., 2016](#)). Therefore, to limit granulation tissue formation, all subsequent implants were created using CT-reconstructed skulls. No granulation tissue and a close fit to the skull were observed in NHP B and NHP M’s post-implantation CT scans ([Fig. 12](#)).

Future studies should aim to quantitatively examine the difference between CT and MRI digitally reconstructed skulls. In situations where CT data are not available, the distortions in the MRI data must be corrected. To correct the MRI data, we recommend applying a gradient distortion correction, which is often performed by default on commercial MRI systems. Furthermore, in situations where MRI data are used to perform high-resolution deep brain navigation and CT data are used to create the implant, an accurate co-registration must be obtained. To perform an accu-

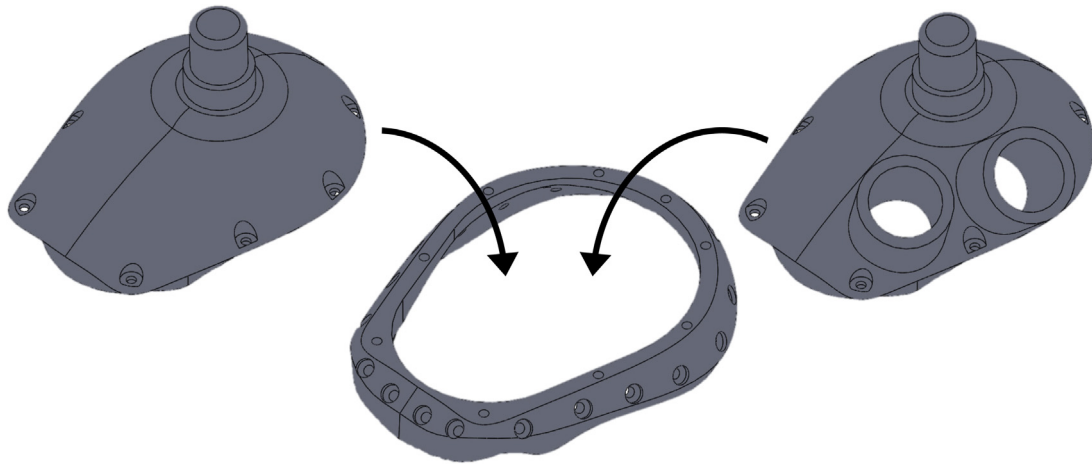


**Fig. 14.** Prototype PEEK “ring and cap” design. The middle ring is screwed to the skull while different customized caps (left and right) can be interchanged.

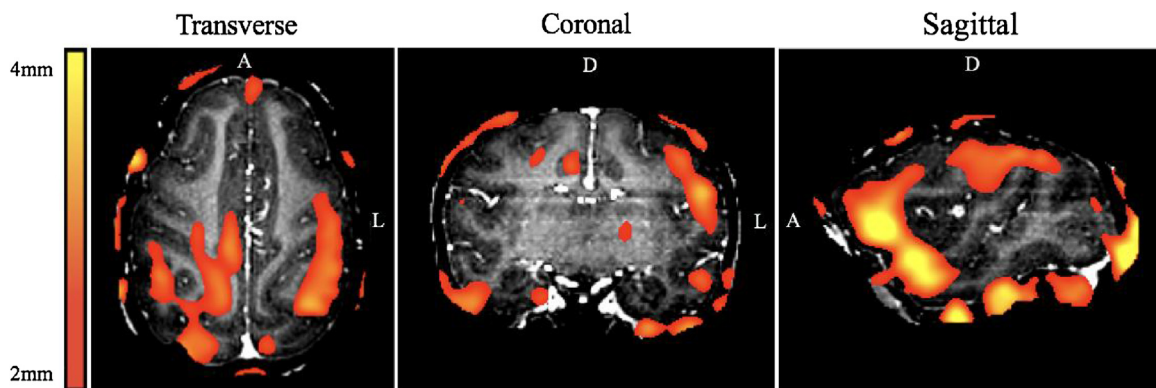


**Fig. 15.** Discrepancies between 3T and 7T MRI in NHP T. Red corresponds to a 2 mm distortion and yellow corresponds to a 4 mm distortion. A = Anterior, D = Dorsal, L = Left. (For interpretation of the references to colour in this figure legend, the reader is referred to the web version of this article.)

rate co-registration, we recommend correcting the MRI data before co-registration.

The breakage of the PEEK screws that attached the headpost to the cap for NHP T was also a concern in the current study. PEEK screws were initially used to hold the headpost to the cap to keep the implant fully MRI compatible. We presumed that six screws in combination with the grooves on the headpost baseplate would be enough to withstand the torque applied by NHP T; however, the screws broke shortly after head fixation was initiated. This motivated us to perform materials testing to determine the relative strengths of the implant components. To do this, a model of the headpost baseplate was cut from a block of PEEK and fastened to a solid surface. Using this model and the actual headpost holder that was used on the primate, we applied crude manual force to various combinations of PEEK or titanium headposts and screws. Though subjective in terms of force application, we found that the PEEK screws broke first when paired with a PEEK headpost or titanium headpost. When the PEEK screws were replaced with titanium screws, the PEEK and titanium headposts withstood maximal force applied by an adult male researcher. When the number of titanium screws was reduced to one, the next thing to fail was the PEEK threading inside the screw hole. This testing, coupled with our experience with NHP T revealed that the weakest points of the cap implant are the PEEK headpost screws, followed by the threading in the headpost screw holes. This shows that the headpost and the cap implant itself are both resistant and that titanium screws should be used for head fixation in large primates. To perform awake head fixation in an MRI, stronger PEEK variants, such

as glass-reinforced or carbon fiber-reinforced PEEK could be used to create the headpost screws. To provide increased resistance to PEEK screw breakage, the cap could also be designed with deeper baseplate ridges, more screws, or a headpost that is continuous with the cap. However, incorporating the headpost into the cap as a continuous piece would not allow the skin to be initially fully sealed following cap implantation. Additionally, a metal headpost holder for behavioural training may cause the PEEK headpost to wear down over time, which is problematic because it would be difficult to replace. A fourth and final possibility for awake MRI head fixation is to incorporate ridges into the sides of the cap to house the tips of bolts that are implemented in an MRI-compatible halo head fixation system (Isoda et al., 2005). This would avoid headpost implantation, but would require small incisions on the animal's skin to access the cap implant.

#### 4.2. Conclusion

Taken together, our implants provided full customizability, increased strength, and reduced surgical invasiveness. These benefits were combined with many modern advances in implant design, including custom-fitting using imaging data, surgical pre-planning, and avoiding the use of acrylic.

There are many future applications for our implant design in basic research, including: acute array implantation, optogenetics, MRI coil implantation, micro-stimulation, and head fixation of an awake primate during an MRI scan. For brain navigation, a fiducial array can be fastened to its own location on the cap or onto a head-

post adaptor (Fig. 8A). As Chen et al. (2017) have noted, it is not yet possible to effectively 3D-print PEEK implants; however, our design has the potential to be 3D-printed from titanium. Using titanium would make the implant stronger and would be useful for labs not concerned with MRI compatibility. In these situations, the potential detrimental effects of titanium's high elastic modulus would have to be considered (Sagomyants et al., 2008). Our implant design also has potential clinical implications by influencing the design of human implants used for neuroprosthetics, deep brain stimulation, and brain-machine interfaces. Though a full cap may be impractical for human applications, the principles of customizability, force distribution, decreased surgical invasiveness, and optimization of skull surface area could be considered.

In conclusion, our custom-fit PEEK cap implants help to advance the field of primate electrophysiology while motivating researchers to adopt safer and more sustainable techniques. It is imperative that future research continues to refine implant design and methodology to ensure high ethical standards and to optimize the scientific contribution of research animals.

### Conflict of interest

Kevin Barker contributed intellectually to the design of the implant and was paid through his company, *Neuronitek* for manufacturing the implants.

### Acknowledgements

This work was supported by the Canadian Institutes of Health Research, Natural Sciences and Engineering Research Council, and Canada Research Chair program grants to J.M.-T. We thank Kim Thomaes, Rhonda Kersten, and Ashley Kirley for their assistance with animal procedures and other members of the J.M.-T. Laboratory for providing writing assistance and proof-reading this manuscript.

### Appendix A. Supplementary data

Supplementary data associated with this article can be found, in the online version, at <https://doi.org/10.1016/j.jneumeth.2018.04.016>.

### References

- Adams, D.L., Economides, J.R., Jocson, C.M., Horton, J.C., 2007. A biocompatible titanium headpost for stabilizing behaving monkeys. *J. Neurophysiol.* 98 (2), 993–1001, <http://dx.doi.org/10.1152/jn.00102.2007>.
- Adams, D.L., Economides, J.R., Jocson, C.M., Parker, J.M., Horton, J.C., 2011. A watertight acrylic-free titanium recording chamber for electrophysiology in behaving monkeys. *J. Neurophysiol.* 106 (3), 1581–1590, <http://dx.doi.org/10.1152/jn.00405.2011>.
- Betelak, K.F., Margiotti, E.A., Wohlford, M.E., Suzuki, D.A., 2001. The use of titanium implants and prosthodontic techniques in the preparation of non-human primates for long-term neuronal recording studies. *J. Neurosci. Methods* 112 (1), 9–20, [http://dx.doi.org/10.1016/S0165-0270\(01\)00442-3](http://dx.doi.org/10.1016/S0165-0270(01)00442-3).
- Borden, P.Y., Ortiz, A.D., Waiblinger, C., Sederberg, A.J., Morrissette, A.E., Forest, C.R., et al., 2017. Genetically expressed voltage sensor ArcLight for imaging large scale cortical activity in the anesthetized and awake mouse. *Neurophotonics* 4 (3), 1–21, <http://dx.doi.org/10.1117/1.NPh.4.3.031212>.
- Buser, D., Schenk, R.K., Steinemann, S., Fiorellini, J.P., Fox, C.H., Stich, H., 1991. Influence of surface characteristics on bone integration of titanium implants. A histomorphometric study in miniature pigs. *J. Biomed. Mater. Res. A* 25 (7), 889–902, <http://dx.doi.org/10.1002/jbm.820250708>.
- Chang, J.C., Hurst, T.L., Hart, D.A., Estey, A.W., 2002. 4-META use in dentistry: a literature review. *J. Prosthet. Dent.* 87 (2), 216–224, <http://dx.doi.org/10.1067/mpd.2002.121584>.
- Chen, X., Possel, J.K., Wacongne, C., van Ham, A.F., Klink, P.C., Roelfsema, P.R., 2017. 3D printing and modelling of customized implants and surgical guides for non-human primates. *J. Neurosci. Methods* 286, 38–55, <http://dx.doi.org/10.1016/j.jneumeth.2017.05.013>.
- Cignoni, P., Callieri, M., Corsini, M., Dellepiane, M., Ganovelli, F., Ranzuglia, G., 2008. Meshlab: an open-source mesh processing tool. *Sixth Eurographics Italian Chapter Conference*, 129–136.
- Dahl, O.E., Garvik, L.J., Lyberg, T., 1994. Toxic effects of methylmethacrylate monomer on leukocytes and endothelial cells in vitro. *Acta Orthop. Scand.* 65 (2), 147–153, <http://dx.doi.org/10.3109/17453679408995423>.
- De Rezende, M.R., Johansson, C.B., 1993. Quantitative bone tissue response to commercially pure titanium implants. *J. Mater. Sci.* 4 (3), 233–239, <http://dx.doi.org/10.1007/BF00122274>.
- Dotson, N.M., Hoffman, S.J., Goodell, B., Gray, C.M., 2017. A large-scale semi-chronic microdrive recording system for non-human primates. *Neuron* 96 (4), 769–782, <http://dx.doi.org/10.1016/j.neuron.2017.09.050>.
- Dunne, N.J., Orr, J.F., 2002. Curing characteristics of acrylic bone cement. *J. Mater. Sci.* 13 (1), 17–22, <http://dx.doi.org/10.1023/A:1013670132001>.
- Eriksson, A.R., Albrektsson, T., 1983. Temperature threshold levels for heat-induced bone tissue injury: a vital-microscopic study in the rabbit. *J. Prosthet. Dent.* 50 (1), 101–107, [http://dx.doi.org/10.1016/0022-3913\(83\)90174-9](http://dx.doi.org/10.1016/0022-3913(83)90174-9).
- Huiskes, R., Weinans, H., Van Rietbergen, B., 1992. The relationship between stress shielding and bone resorption around total hip stems and the effects of flexible materials. *Clin. Orthop.*, 124–134, <http://dx.doi.org/10.1097/00003086-199201000-00014>.
- Hunter, A., Archer, C.W., Walker, P.S., Blunn, G.W., 1995. Attachment and proliferation of osteoblasts and fibroblasts on biomaterials for orthopaedic use. *Biomaterials* 16 (4), 287–295, [http://dx.doi.org/10.1016/0142-9612\(95\)93256-D](http://dx.doi.org/10.1016/0142-9612(95)93256-D).
- Isoda, M., Tsutsui, K.I., Katsuyama, N., Naganuma, T., Saito, N., Furusawa, Y., et al., 2005. Design of a head fixation device for experiments in behaving monkeys. *J. Neurosci. Methods* 141 (2), 277–282, <http://dx.doi.org/10.1016/j.jneumeth.2004.07.003>.
- Johnston, J.M., Cohen, Y.E., Shirley, H., Tsunada, J., Bennis, S., Christison-Lagay, K., Veeder, C.L., 2016. Recent refinements to cranial implants for rhesus macaques (*Macaca mulatta*). *Lab Anim.* 45 (5), 180, <http://dx.doi.org/10.1038/labana.997>.
- Katzer, A., Marquardt, H., Westendorf, J., Wening, J.V., Von Foerster, G., 2002. Polyetheretherketone—cytotoxicity and mutagenicity in vitro. *Biomaterials* 23 (8), 1749–1759, [http://dx.doi.org/10.1016/S0142-9612\(01\)00300-3](http://dx.doi.org/10.1016/S0142-9612(01)00300-3).
- Lanz, F., Lanz, X., Scherly, A., Moret, V., Gaillard, A., Gruner, P., et al., 2013. Refined methodology for implantation of a head fixation device and chronic recording chambers in non-human primates. *J. Neurosci. Methods* 219 (2), 262–270, <http://dx.doi.org/10.1016/j.jneumeth.2013.07.015>.
- Lau, J.C., Khan, A.R., Zeng, T.Y., MacDougall, K.W., Parrent, A.G., Peters, T.M., 2018. Quantification of local geometric distortion in structural magnetic resonance images: application to ultra-high fields. *Neuroimage* 168, 141–151, <http://dx.doi.org/10.1016/j.neuroimage.2016.12.066>.
- Leavitt, M.L., Pieper, F., Sachs, A.J., Martinez-Trujillo, J.C., 2017. Correlated variability modifies working memory fidelity in primate prefrontal neuronal ensembles. *Proc. Natl. Acad. Sci. U. S. A.* 114 (12), <http://dx.doi.org/10.1073/pnas.1619949114>.
- Lisberger, S.G., Westbrook, L.E., 1985. Properties of visual inputs that initiate horizontal smooth pursuit eye movements in monkeys. *J. Neurosci.* 5 (6), 1662–1673, <http://www.jneurosci.org/content/jneuro/5/6/1662.full.pdf>.
- McAndrew, R.M., VanGilder, J.L., Naufel, S.N., Tillery, S.H., 2012. Individualized recording chambers for non-human primate neurophysiology. *J. Neurosci. Methods* 207 (1), 86–90, <http://dx.doi.org/10.1016/j.jneumeth.2012.03.014>.
- McNeel, R., 2015. Rhinoceros (NURBS modeling for Windows: <http://www.rhino3d.com>).
- Mendoza-Halliday, D., Torres, S., Martinez-Trujillo, J.C., 2014. Sharp emergence of feature-selective sustained activity along the dorsal visual pathway. *Nat. Neurosci.* 17, 1255–1262, <http://dx.doi.org/10.1038/nn.3785>.
- Mitz, A.R., Tsujimoto, S., MacLarty, A.J., Wise, S.P., 2009. A method for recording single-cell activity in the frontal-pole cortex of macaque monkeys. *J. Neurosci. Methods* 177 (1), 60–66, <http://dx.doi.org/10.1016/j.jneumeth.2008.09.032>.
- Mueller, J.K., Grigsby, E.M., Prevosto III, V., Petraglia, F.W., Rao, H., Deng, Z.D., et al., 2014. Simultaneous transcranial magnetic stimulation and single-neuron recording in alert non-human primates. *Nat. Neurosci.* 17 (8), 1130–1136, <http://dx.doi.org/10.1038/nn.3751>.
- Mulliken, G.H., Bichot, N.P., Ghaadooshahy, A., Sharma, J., Kornblith, S., Philcock, M., Desimone, R., 2015. Custom-fit radiolucent cranial implants for neurophysiological recording and stimulation. *J. Neurosci. Methods* 241, 146–154, <http://dx.doi.org/10.1016/j.jneumeth.2014.12.011>.
- Nakagawa, K., Saita, M., Ikeda, T., Hirota, M., Park, W., Lee, M.C.I., Ogawa, T., 2015. Biocompatibility of 4-META/MMA-TBB resin used as a dental luting agent. *J. Prosthet. Dent.* 114 (1), 114–121, <http://dx.doi.org/10.1016/j.prosdent.2014.10.016>.
- Niki, Y., Matsumoto, H., Otani, T., Suda, Y., Toyama, Y., 2001. Metal ion concentrations in the joint fluid immediately after total knee arthroplasty. *Mod. Rheumatol.* 11 (3), 192–196, <http://dx.doi.org/10.3109/s101650170003>.
- Nummela, S.U., Coop, S.H., Cloherty, S.L., Boisvert, C.J., Leblanc, M., Mitchell, J.F., 2017. Psychophysical measurement of marmoset acuity and myopia. *Dev. Neurobiol.* 77 (3), 300–313, <http://dx.doi.org/10.1002/dneu.22467>.
- Ormianer, Z., Laufer, B.Z., Nissan, J., Gross, M., 2000. An investigation of heat transfer to the implant-bone interface related to exothermic heat generation during setting of autopolymerizing acrylic resins applied directly to an implant abutment. *Int. J. Oral Maxillofac. Implants* 15 (6), [http://www.quintpub.com/journals/omi/fulltext.php?article\\_id=286](http://www.quintpub.com/journals/omi/fulltext.php?article_id=286).
- Overton, J.A., Cooke, D.F., Goldring, A.B., Lucero, S.A., Weatherford, C., Recanzone, G.H., 2017. Improved methods for acrylic-free implants in nonhuman primates

- for neuroscience research. *J. Neurophysiol.* 118 (6), 3252–3270, <http://dx.doi.org/10.1152/jn.00191.2017>.
- Pfingst, B.E., Albrektsson, T., Tjellström, A., Miller, J.M., Zappia, J., Xue, X., Weiser, F., 1989. Chronic skull-anchored percutaneous implants in non-human primates. *J. Neurosci. Methods* 29 (3), 207–216, [http://dx.doi.org/10.1016/0165-0270\(89\)90145-3](http://dx.doi.org/10.1016/0165-0270(89)90145-3).
- Rho, J.Y., Ashman, R.B., Turner, C.H., 1993. Young's modulus of trabecular and cortical bone material: ultrasonic and microtensile measurements. *J. Biomech.* 26 (2), 111–119, [http://dx.doi.org/10.1016/0021-9290\(93\)90042-D](http://dx.doi.org/10.1016/0021-9290(93)90042-D).
- Rosset, A., Spadola, L., Ratib, O., 2004. OsiriX: an open-source software for navigating in multidimensional DICOM images. *J. Digit. Imaging* 17 (3), 205–216, <http://dx.doi.org/10.1007/s10278-004-1014-6>.
- Sagomonyants, K.B., Jarman-Smith, M.L., Devine, J.N., Aronow, M.S., Gronowicz, G.A., 2008. The in vitro response of human osteoblasts to polyetheretherketone (PEEK) substrates compared to commercially pure titanium. *Biomaterials* 29 (11), 1563–1572, <http://dx.doi.org/10.1016/j.biomaterials.2007.12.001>.
- Tremblay, S., Pieper, F., Sachs, A., Martinez-Trujillo, J., 2015. Attentional filtering of visual information by neuronal ensembles in the primate lateral prefrontal cortex. *Neuron* 85 (1), 202–215, <http://dx.doi.org/10.1016/j.neuron.2014.11.021>.
- Treon, J.F., Sigmon, H., Wright, H., Kitzmiller, K.V., 1949. The toxicity of methyl and ethyl acrylate. *J. Ind. Hyg. Toxicol.* 31 (6), 317–326.